

# A method for large-scale synthesis of Al-doped TiO<sub>2</sub> nanopowder using pulse-modulated induction thermal plasmas with time-controlled feedstock feeding

メタデータ	言語: eng 出版者: 公開日: 2017-10-03 キーワード (Ja): キーワード (En): 作成者: メールアドレス: 所属:
URL	<a href="http://hdl.handle.net/2297/37535">http://hdl.handle.net/2297/37535</a>

# Method for large-scale synthesis of Al-doped TiO<sub>2</sub> nanopowder using pulse-modulated induction thermal plasmas with time-controlled feedstock feeding

Naoto Kodama<sup>†</sup>, Yasunori Tanaka<sup>†</sup>, K Kita, Y Uesugi,  
T Ishijima, S Watanabe<sup>‡</sup>, K Nakamura<sup>‡</sup>

Faculty of Electrical Engineering and Computer Science, Kanazawa University,  
Kakuma, Kanazawa 920-1192, JAPAN

<sup>‡</sup>Research Center for Production & Technology, Nisshin Seifun Group Inc., 5-3-1  
Tsurugaoka, Fujimino 356-8511, JAPAN

E-mail: me131027@ec.t.kanazawa-u.ac.jp, tanaka@ec.t.kanazawa-u.ac.jp

**Abstract.** A unique large-scale synthesis method for Al-doped TiO<sub>2</sub> nanopowder was developed using 20-kW Ar-O<sub>2</sub> pulse-modulated induction thermal plasmas (PMITP) with time-controlled feedstock feeding (TCFF). This PMITP-TCFF method is characterized by intermittent feedstock powder feeding synchronized with modulated power of the PMITP. The method enables heavy-load feeding of raw material powder to the thermal plasmas for complete evaporation. Synthesized nanopowder was analyzed using different methods including FE-SEM, XRD, BF-TEM, TEM/EDX mapping, XPS, and spectrophotometry. Results showed that Al-doped TiO<sub>2</sub> nanopowder can be synthesized with mean diameters of 50–60 nm. The Al doping in TiO<sub>2</sub> was confirmed from the constituent structure in XRD spectra, the uniform presence of Al on the nanopowder in TEM/EDX mapping, the chemical shift in XPS spectra, and the absorption edge shift in the optical property. The production rate of Al-doped TiO<sub>2</sub> nanopowder was estimated as 400 g h<sup>-1</sup>.

PACS numbers: 52.50.Dg, 52.80.Pi, 61.43.Gt, 61.72.Ww

Submitted to: *J. Phys. D: Appl. Phys.*

<sup>†</sup> To whom correspondence should be addressed (me131027@ec.t.kanazawa-u.ac.jp, tanaka@ec.t.kanazawa-u.ac.jp)

## 1. Introduction

Nanopowder or nanoparticles are anticipated as promising next-generation elements for use in various applications such as in electronics, energy, and environmental fields. Titanium dioxide (TiO<sub>2</sub>) nanopowder is continually receiving attention for use as photocatalysts [1], photonic crystals [2], photovoltaic cells [3], and gas sensors [4]. It is also anticipated for use as a strong deoxidation material used for producing hydrogen gas from water for fuel cells [5]. In fact, TiO<sub>2</sub> is well known to work as a photocatalyst under ultraviolet light because of its wide energy band gap. This problem can be improved by metallic-ion doping of TiO<sub>2</sub> materials because the energy levels of the doped material in the energy band gap of TiO<sub>2</sub> improve their visible light absorption efficiency [6]–[8]. Another application of such metallic-ion doped TiO<sub>2</sub> nanoparticles is in the biomedical field [9, 10]. Reportedly, Al-doped TiO<sub>2</sub> nanoparticles have protein adsorption ability, which is expected to be effective for skin care, specifically for atopic dermatitis [10]. This adsorption effect might be attributed to the fact that Al-doped TiO<sub>2</sub> nanoparticles are positively charged in water dispersion, which can attract inflammatory proteins with a negatively charged functional group. For such biomedical applications, an effective method for mass production of Al-doped TiO<sub>2</sub> nanopowder without impurity is strongly desired from an industrial view point. Nevertheless, it has not yet been developed for such metallic-ion doped TiO<sub>2</sub> nanopowder without impurity contamination.

Various types of nanopowder synthesis methods have been developed. Among them, the inductively coupled thermal plasma (ICTP) method is a useful technique to synthesize nanoparticles of various kinds [11]–[18]. It provides one-step direct processing including rapid evaporation of injected raw materials, and enables rapid cooling of evaporated materials. It can offer nanoparticles in non-equilibrium or metastable phase. The most important benefit of this method is that it can fundamentally provide nanoparticles without any impurity. Several studies have examined the synthesis of TiO<sub>2</sub> nanoparticles using a steady-state type of inductively coupled thermal plasma (ICTP). They have mainly investigated control of its particle size and phase constituent [13, 14, 18]. However, some issues persist: the difficulty in controlling the synthesized particle size, and also the lower production rate from the instability of ICTP sustainability during heavy-load feeding of feedstock.

The authors recently developed a new synthesis method of large amounts of pure oxide nanopowder without contamination using pulse-modulated induction thermal plasma (PMITP) with time-controlled feeding of feedstock (TCFF) [19]–[21]. The PMITP was developed by our group to control the temperature and chemical activity fields in thermal plasmas using coil-current modulation [23, 24]. In addition to this, our group recently developed a method for feedstock powder injection, in which the feedstock powder is supplied intermittently to the thermal plasma periodically, in synchronization with the coil-current modulation of the PMITP. This intermittent and synchronized feeding of feedstock is a time-controlled feedstock feeding (TCFF) method [21, 22]. The TCFF was combined with the PMITP for nanopowder synthesis. This PMITP–

TCFF method accommodates heavy-load feeding of feedstock powder, thereby providing complete evaporation. In our previous work, the PMITP-TCFF method developed as explained above was adopted to synthesize pure TiO<sub>2</sub> nanopowder for mass production. Results show that this method using a 20-kW PMITP supported a production rate of about 500 g h<sup>-1</sup> of pure TiO<sub>2</sub> nanopowder with mean particle diameter of about 43 nm [21].

This paper describes the experimental results of trial adoption of our uniquely-developed PMITP-TCFF method to synthesize large amounts of Al-doped TiO<sub>2</sub> nanopowder, as well as TiO<sub>2</sub> nanopowder. Mass production of metallic-ion doped nanopowder is a key issue in nanotechnology fields for various applications including skincare creams for anti-atopic dermatitis. The synthesized nanopowder was analyzed using different methods, including FE-SEM, to assess the morphology of nanoparticles and their size distribution, XRD and TEM/EDX mapping for the crystal phase composition of the particle and the estimation of Al doping, XPS for estimation of the chemical-bonding state in the particles, and spectrophotometry for optical property evaluation. In addition, the effects of the degree of coil-current modulation were particularly investigated in the synthesized nanopowder. The Al-doped TiO<sub>2</sub> nanopowder was synthesized using our originally developed PMITP-TCFF method. The Al-doped TiO<sub>2</sub> nanopowder production rate was finally estimated as about 400 g h<sup>-1</sup> using a 20-kW PMITP, which is about 10 times higher than that attained using the conventional method with steady-state induction thermal plasmas.

## 2. Methodology of a large-scale nanopowder synthesis system

Here, our developed method is described briefly for synthesis of large amounts of nanopowders using a PMITP-TCFF, although it has been described in our previous paper [21].

We have developed a pulse-modulated induction thermal plasma (PMITP) system. The PMITP is sustained by the coil current on the order of several hundreds of amperes, the amplitude of which is modulated into a rectangular waveform. Such modulation of the coil current can repetitively produce a high-temperature field during the ‘on-time’ and a low-temperature field during ‘off-time’ in thermal plasmas. Figure 1 portrays the coil current modulated into a rectangular waveform and the definition of modulation parameters. As presented in figure 1, the on-time is the time period with the higher current level (HCL), although the off-time means the time period with the lower current level (LCL). We have also defined a shimmer current level (SCL) as a ratio of LCL to HCL. In addition, the duty factor (DF) has been defined as the ratio of on-time in one modulation period. A condition of 100%SCL or 100%DF corresponds to the non-modulation condition. A lower SCL condition is equivalent to a condition with a larger modulation degree.

Figure 2 presents our developed methodology for the synthesis of large amounts of nanopowder using a pulse-modulated induction thermal plasma (PMITP) with time-

controlled feeding of the feedstock (TCFF). As explained earlier, the PMITP can produce a higher temperature field and a lower temperature field repetitively according to the coil current modulation. To this PMITP, the feedstock solid powder is supplied from a powder feeder through a powder feeding tube with Ar carrier gas from the top of the plasma torch head to the PMITP. Furthermore, a high speed valve is installed on the tube between the powder feeder and the plasma torch. This high-speed solenoid valve has a response time of 2 ms to open and close. Setting the open and close timing of the valve can control the actual timing and the time length of the powder feeding. The right hand side of figure 2 shows the timing chart of the coil current modulation, switching signal of the solenoid valve, and the actual powder feeding. For synthesis of large amounts of nanopowder, heavy-load feeding of feedstock is necessary without extinction of the plasma or incomplete evaporation of the feedstock. In our method, the feedstock powder is controlled to be fed intermittently and synchronously only during the high-temperature period in the on-time of the PMITP. This synchronized powder feeding can be executed easily by controlling the delay time  $t_d$  for the opening timing of the valve in reference to the pulse modulation signal of the PMITP. In the actual experiment, the powder reaches to the PMITP in a finite time after inputting the opening signal to the solenoid valve. This finite time was measured in our previous work as another delay time  $t_{adt}$  of 6–8 ms [21]. Therefore, the actual total delay time is  $(t_d + t_{adt}) \simeq (t_d + 7)$  ms before the powder is actually injected to the PMITP. The intermittent and synchronized feedstock feeding can be performed while taking account of this total delay time  $(t_d + 7)$  ms.

The injected feedstock powder with heavy-load is evaporated rapidly, completely, and efficiently in a high temperature plasma during the on-time of the PMITP because of higher power injection to the PMITP. The feedstock injection is stopped by closing the solenoid valve during the successive off-time. In the off-time, the evaporated feedstock material is cooled down rapidly because the thermal plasma temperature decreases as a result of the decreased input power to the PMITP. This rapid cooling might promote particle nucleation from evaporated Ti and O atom in vapour in the PMITP. Nucleated particles are transported downstream of the PMITP torch with particle growth. Downstream of the PMITP torch, the quenching gas is injected in the radial direction. Such a quenching gas injection cools the evaporated material further to restrain the synthesized particle growth. Then, in the successive on-time, the input power increases to rebuild high-temperature thermal plasma for the subsequent powder injection. In this way, the PMITP-TCFF method described above can create effective vaporization of the feedstock and support the effective cooling of the evaporated material. It enables synthesis of large amounts of nanopowder with a high production rate.

### 3. Experimental

#### 3.1. Experimental arrangements

Figure 3 shows the whole nanopowder synthesis system used in the present experiments. This nanopowder synthesis system has three main parts: an rf power source, a synchronized intermittent feedstock feeding system, and the plasma torch and the chamber. The rf power source is operated as a half-bridge inverter power supply with a metal-oxide semiconductor field emission transistor (MOSFET) at rated power of 30 kW. Its driving fundamental frequency was 450 kHz. This power supply can modulate the output electric current amplitude of several hundreds of amperes into a rectangular waveform according to the modulation signal from the pulse generator.

The synchronized intermittent feedstock feeding system has the transistor-transistor logic (TTL) signal circuit, a delayed trigger signal circuit, the high-speed solenoid valve on the powder feeding tube, and the powder feeder. The TTL signal circuit translates a modulation signal of 0–10 V from the pulse generator for the MOSFET gate signal circuit to a TTL signal of 0–5 V. This TTL signal is inputted to the delayed trigger circuit, which outputs a TTL signal with a given delay time of  $t_d$  against the modulation signal. This delayed signal is used to open and close the high speed solenoid valve for powder feeding.

The plasma torch is configured identically to that used in our previous work. Its details were described in elsewhere [23, 24]. The plasma torch has two coaxial quartz tubes. The interior quartz tube has 70 mm inner diameter; its length is 370 mm. An argon–oxygen gas mixture was supplied as a sheath gas along the inside wall of the interior quartz tube from the top of the plasma torch. A powder mixture of titanium (Ti) and aluminium (Al) raw materials was fed using a powder feeder with Ar carrier gas through a water-cooled tube probe. The water-cooled tube probe was inserted from the top of the plasma torch head, as depicted in figure 3. Downstream of the plasma torch, quenching gas was supplied to cool down the evaporated material to promote nucleation. Further downstream, the water-cooled chambers were installed vertically and then horizontally, as depicted in figure 3. The total length of the vertical chamber is 600 mm; its inner diameter is 130 mm. Similarly, the total length of the horizontal chamber is 600 mm; its inner diameter is 130 mm. Further downstream of the horizontal chamber, a powder-collecting filter and the collecting chamber are set up. A vacuum pump is set up further downstream.

#### 3.2. Experimental conditions

Table 1 summarizes the experimental conditions in the present work. The time-averaged input power was fixed at 20 kW to the inverter power supply. This inverter power supply in the experiment was a semiconductor power supply with fundamental frequency of 450 kHz. This power supply was measured to have high power conversion efficiency of more than 95%. Therefore, the greater than 19 kW was outputted from the power supply.

The instantaneous input power  $P_{\text{in}}(t)$  was also changed periodically with time according to the coil current modulation. For 80%SCL-80%DF condition for example, the quantity  $P_{\text{in}}(t)$  increased gradually with a time constant of about 1.6 ms during the on-time and reached 28 kW, although it decreased with a time constant of 2.0 ms during the off-time, reaching 10 kW. The modulation cycle was fixed at 15 ms. The reason to select the modulation cycle of 15 ms is attributed to the fact that the residence time of the reactant vapour was estimated as 10–20 ms according to the gas flow velocity calculation by numerical thermo-fluid simulation [19]. It is expected for this time period to provide sufficient evaporation of the injected powders in the high-temperature region in the plasma during the on-time, and successive rapid cooling of the plasma tail during the off-time. The DF of the modulated coil current was fixed at 80%. Only the modulation degree, i.e. the shimmer current level (SCL), was changed to 60%, 70% and 80%.

The total sheath gas flow rate was fixed at 100 L min<sup>-1</sup> (litres per minute). The O<sub>2</sub> gas admixture ratio to Ar was set at 10 mol% in the sheath gas in gas flow rate. The Ar quenching gas flow rate was fixed at 50 L min<sup>-1</sup>. The chamber pressure was fixed at 300 Torr (=40 kPa). The feedstock was a mixture of 5 wt%Al (ALE11PB; Kojundo Chemical Lab. Co. Ltd.) and 95wt%Ti (TILOP-45; Osaka Titanium Technologies Co., Ltd.) powder. The mean diameter of Al raw powder is about 3 μm, whereas that of Ti raw powder was 27 μm. The feedstock was fed into the plasma torch using a rotary powder feeder with Ar carrier gas. The Ar carrier gas flow rate was fixed at 4 L min<sup>-1</sup>. The feeding rate of the feedstock  $g_{\text{pow}}$  was found to be 19 g min<sup>-1</sup> at 60%SCL, 12 g min<sup>-1</sup> at 70%SCL and 12 g min<sup>-1</sup> at 80%SCL, respectively, by weight measurements after each of the experiments. These powder feeding rates are much higher than those in other conventional nanoparticle synthesis methods described in the literature. They used induction thermal plasmas of several tens of kilowatts [6, 14]. The feedstock was fed intermittently with a high-speed solenoid valve that was synchronized with the coil current modulation with delay time  $t_d$  of 6 ms. The open time and close time of the high-speed solenoid valve were, respectively, 12 ms and 3 ms. Nanopowder synthesis experiments were conducted for 5 min for each of the experiments under three SCL conditions. After each experiment, synthesized powder was collected at the filter. Morphology and size distribution of synthesized powder were analyzed using a field emission scanning electron microscope (FE-SEM) and a bright-field transmission electron microscope (BF-TEM). The FE-SEM analyses were carried out on a JEOL JSM-6700F operated at 5 kV. The crystal phase composition was identified using X-ray diffraction (XRD) spectroscopy. The XRD measurements were carried out on a Rigaku RINT-Ultima III operated at 40 kV and 40 mA. The element distribution of Ti, O and doped Al atom was mapped using TEM / energy dispersive X-ray (EDX) spectrometry. The chemical-bonding state of in the synthesized powder was estimated using X-ray photo-electron spectroscopy (XPS) on a carbon-tape. The XPS measurements were carried out on a Thermo VG Scientific Sigma Probe using monochromatic AlK<sub>α</sub> radiation. The calibration of peak positions was made using the C 1s line at 285 eV after experimental acquisitions, because the carbon originated from

carbon-tape was well detected. The spot-size of XPS measurements were  $400\ \mu\text{m}$  with pass energy of 600 eV. The optical property of the synthesized powders were evaluated by using a Hitachi U-4100 spectrophotometer. The final nanopowder production rate was estimated from the weight of the synthesized powder, together with the fraction of nanopowder from the analysis described above.

## 4. Results and discussions

### 4.1. SEM images and particle size distribution of synthesized powder

Figure 4 presents FE-SEM images of feedstock and the synthesized nanopowder collected at the filter in different SCL conditions. The feedstock Ti powder has mean diameter around  $27\ \mu\text{m}$  with various shapes. However, most of synthesized particles were found to have a size of 100 nm or less in any of the three SCL conditions in the present experiments. Therefore, nanosized particles were produced despite heavy-load feeding of the feedstock using our developed method. The shapes of the synthesized particles were also observed to be almost spherical for these three conditions, which implies that nanoparticles were synthesized and grown in gas phase rather than on the surface of the filter or the wall.

From these FE-SEM images, the particle size distributions were evaluated by measuring diameters of 200 randomly selected particles. Figure 5 depicts the size distribution of particles synthesized using the PMITP-TCFF method with three SCL conditions. More than 90% of the synthesized particles are nanoparticles of less than 100 nm diameter for three SCL conditions. The particle mean diameter  $\bar{d}$ , median  $d_{50}$ , and standard deviation  $\sigma$  for the synthesized nanopowder were calculated from the particle size distribution. The quantities  $\bar{d}$ ,  $d_{50}$  and  $\sigma$  are also presented in figure 5. These magnitudes  $\bar{d}$  and  $\sigma$  are shown as a function of the SCL in figure 6. The  $\bar{d}$  refers to the left vertical axis, whereas  $\sigma$  to the right vertical axis in this figure. This figure suggests that lower SCL, which leads a larger modulation degree, provides nanoparticles with smaller  $\bar{d}$ . The quantity  $\bar{d}$  decreases from 68 nm to 53 nm with reduction of SCL from 80% to 60%. An interesting point is that the  $\bar{d}$  for 60%SCL is smaller than those for 70%SCL and 80%SCL, although the condition 60%SCL has a higher feeding rate  $g_{\text{pow}}$  of  $19\ \text{g min}^{-1}$ , whereas  $g_{\text{pow}} = 12\ \text{g min}^{-1}$  for 80%SCL and 70%SCL. Generally, a higher  $g_{\text{pow}}$  often leads to a larger  $\bar{d}$  of synthesized particles because a higher  $g_{\text{pow}}$  forms a higher density vapour cloud in the thermal plasma to promote particle growth. Synthesized particles were also collected in the upstream chamber and the downstream chamber. More than 90% of the synthesized particles collected in the upstream and downstream chamber have diameters less than 100 nm. No unmelted and non-vaporized feedstocks were found for 80% and 70%SCL with  $g_{\text{pow}} = 12\ \text{g min}^{-1}$  conditions. This fact demonstrates no micro-sized powder such as unmelted and non-vaporized powder was synthesized for 80% and 70%SCL with  $g_{\text{pow}} = 12\ \text{g min}^{-1}$  conditions.

Based on these results and weight measurements of the synthesized powder, the

production rates of nanopowder were estimated as more than 400 g h<sup>-1</sup> under  $g_{\text{pow}} = 12$  g min<sup>-1</sup> condition (80%SCL and 70%SCL), for example, using the 20-kW PMITP. This production rate value is 10–20 times higher than those obtained using the conventional thermal plasma method reported in the literature [6, 14]. This important benefit of our developed method, large-scale synthesis of nanopowder, must be emphasized.

#### 4.2. Element distribution analysis of synthesized nanoparticles using BF-TEM & TEM/EDX mapping

This study specifically examines the large-scale synthesis of Al-doped TiO<sub>2</sub> nanopowder. In this case, Al doping is one vital factor to characterize synthesized nanopowder. Figure 7 presents BF-TEM images and TEM/EDX mapping results of synthesized nanopowder collected at the filter. Panel (a) shows the result for condition of 80%SCL with a powder feed range  $g_{\text{pow}}$  of 12 g min<sup>-1</sup>, whereas panel (b) shows the result of the condition 70%SCL and  $g_{\text{pow}}=12$  g min<sup>-1</sup>. Finally, panel (c) shows the results for the condition 60%SCL and  $g_{\text{pow}}=19$  g min<sup>-1</sup>. Each panel has a BF-TEM image and Ti, O, Al element distributions. Magnifications of TEM images and TEM/EDX mapping are different in each panel. From the BF-TEM images, results show that spherical nanoparticles without mesopores were synthesized for these three SCL conditions. The TEM/EDX mapping shows that an Al element was detectable, and that it was distributed almost uniformly in the synthesized particles in the same manner as Ti and O for 80%SCL and 70%SCL, which means that elemental Al might be distributed almost uniformly on the synthesized TiO<sub>2</sub> nanoparticles even by our developed PMITP-TCFF method with heavy-load feeding of feedstock, together with consideration from the XRD and XPS analysis results as described later.

#### 4.3. Chemical composition assessment of synthesized Al-doped TiO<sub>2</sub> nanopowder using XRD spectra analysis

An X-ray diffraction (XRD) analysis was made to study the crystallographic structure and chemical composition of the synthesized nanoparticles. Figure 8 portrays XRD spectra for the synthesized nanopowder collected at the filter. Panel (a) shows the result for the condition of 80%SCL, whereas panel (b) corresponds to the result for 70%SCL, and panel (c) is that for 60%SCL. The designation ‘A’ in these figures indicates that the specified XRD spectral line arises from TiO<sub>2</sub> in anatase form; the designation ‘R’ denotes the lines originating from the TiO<sub>2</sub> in rutile form. Panel (d) shows reference XRD peaks for feedstock and synthesized crystal materials: Ti, Al, Al<sub>2</sub>O<sub>3</sub> and TiO<sub>2</sub> in rutile and anatase phases.

From these figures, the synthesized nanopowder was confirmed clearly as containing mainly rutile and anatase-TiO<sub>2</sub> crystal for three SCL conditions. The weight fraction

$f_A$  of anatase-TiO<sub>2</sub> in the synthesized nanopowder can be estimated from

$$f_A = \frac{1}{1 + 1.26 \frac{I_{R(110)}}{I_{A(101)}}}, \quad (1)$$

where  $I_{R(110)}$  represents the intensity of the (110) reflection of rutile at  $2\theta=27.4^\circ$ , and  $I_{A(101)}$  stands for the intensity of the (101) reflection of anatase at  $2\theta=25.3^\circ$ . Here,  $f_A$  were estimated as about 40 wt% for the 80%SCL condition, 35 wt% for the 70%SCL condition and 40 wt% for the 60%SCL condition. These values of  $f_A$  are lower for the photocatalyst [25]. The lower  $f_A$  and lower photocatalysis characteristics are useful for application to skin care cream [10]. The  $f_A$  in the synthesized nanopowder can be controlled by changing the O<sub>2</sub> concentration in nanopowder processing [13, 26]. The most important feature to be emphasized in the obtained XRD spectra is that no Ti, Al or Al<sub>2</sub>O<sub>3</sub> peaks were detected in nanopowder for 80%SCL and 70%SCL. This result shows that Ti, Al and Al<sub>2</sub>O<sub>3</sub> bulk particles in feedstock were evaporated completely in the high-temperature region of the PMITP, and that Ti was oxidized completely in a highly reactive field to generate TiO<sub>2</sub> crystal. In addition to these XRD spectra, Al or Al<sub>2</sub>O<sub>3</sub> crystal rarely exists in the synthesized particles according to EDX mapping results described in the previous section. This result suggests that Al elements might be doped in TiO<sub>2</sub> nanopowder synthesized using our developed PMITP-TCFF method. However, Al and Ti peaks were detected in the case of 60%SCL and  $g_{\text{pow}} = 19 \text{ g min}^{-1}$ . This might be the result of heavy-load feeding. Therefore, the remaining Al and Ti are present in the synthesized nanopowder.

#### 4.4. Chemical binding state in synthesized Al-doped TiO<sub>2</sub> nanopowder by XPS spectra analysis

The X-ray photo-electron spectroscopy (XPS) was used to measure the elemental composition, chemical state and electronic state of the elements on the surface of the synthesized nanoparticles.

Figure 9 (a) portrays the XPS analysis result for Ti 2p region between 455 eV and 470 eV for the synthesized Al-doped TiO<sub>2</sub> nanopowder.

For comparison, the result for commercial pure-TiO<sub>2</sub> nanopowder (P-25; Degussa) and the result for non-doped pure TiO<sub>2</sub> nanopowder synthesized using our PMITP-TCFF method are presented in figure 9. The non-doped pure TiO<sub>2</sub> nanopowder was synthesized in almost identical conditions with 80%SCL-80%DF and  $g_{\text{pow}}=12 \text{ g min}^{-1}$ , except for raw material without Al powder. The neutralizer was also used to prevent nanoparticles from charging up during the XPS measurement. This figure shows Ti 2p<sub>3/2</sub> and Ti 2p<sub>1/2</sub> peaks for analysis. The commercial pure TiO<sub>2</sub> and pure TiO<sub>2</sub> nanopowder synthesized using the PMITP-TCFF method has almost the same binding energy of 459.30–459.60 eV for Ti 2p<sub>3/2</sub>, and 465.00 eV for Ti 2p<sub>1/2</sub>. These correspond to the binding energy for electrons from the 2p orbit in Ti (IV) in TiO<sub>2</sub>. However, the chemical shifts clearly occurred for Ti 2p<sub>1/2</sub> and Ti 2p<sub>3/2</sub> peaks by the intended addition of Al

elements. For example, this chemical shift is clearly visible from 459.30 eV to 459.60 eV for Ti 2p<sub>3/2</sub> peak in case of Al addition under the condition of 80%SCL and  $g_{\text{pow}}=12$  g min<sup>-1</sup>. This chemical shift is increased further from 459.60 eV to 460.20 eV with reduction of SCL from 80% to 70%, i.e. a larger modulation in the PMITP. These results imply that the Al element was possibly doped in TiO<sub>2</sub>. A higher amount of Al doping might be obtained for reduced SCL. However, the chemical shift to lower binding energy occurred for Ti 2p<sub>3/2</sub> to 457.80 eV in the condition of 60%SCL and  $g_{\text{pow}}=19$  g min<sup>-1</sup>, which might be true because of oxygen deficiency attributable to rich Ti vapour arising from a higher  $g_{\text{pow}}$ . That oxygen deficiency produces Ti<sub>2</sub>O<sub>3</sub> crystals in 60%SCL and  $g_{\text{pow}}=19$  g min<sup>-1</sup> condition.

Figure 9 (b) portrays the XPS analysis result for Al 2p region between 70 eV and 80 eV for the synthesized Al-doped TiO<sub>2</sub> nanopowder. The binding energies around 74.81 eV (condition of 80%SCL), 75.77 eV (condition of 70%SCL) and 73.24 eV (condition of 60%SCL) correspond to Al 2p of Al<sup>3+</sup>, Al 2p<sub>2/3</sub> of Al<sup>3+</sup> and Al 2p of Al<sup>3+</sup>, respectively. They probably indicate that Al<sup>3+</sup> ion exist in TiO<sub>2</sub> crystal and possible formation of the Al-O-Ti chemical bond in the TiO<sub>2</sub> lattice. In addition, they may indicate that Al-doped TiO<sub>2</sub> nanopowder was positively charged due to Al<sup>3+</sup> ion doping [27]. Actually, the Al-doped TiO<sub>2</sub> nanoparticles could be dispersed in the purified water, while TiO<sub>2</sub> nanoparticles were settled down.

#### 4.5. Optical property of synthesized Al-doped TiO<sub>2</sub> nanopowder by spectrophotometric analysis

The metal-ion doping generally changes the optical property of nanopowders. Influence of Al doping to TiO<sub>2</sub> nanopowder was evaluated for the optical property of the synthesized nanopowder by a spectrophotometer for solid powder. Figure 10 shows the integrated total diffuse reflectivity %R for Al-doped TiO<sub>2</sub> synthesized using the PMITP-TCFF method, and then also that for commercial pure-TiO<sub>2</sub> nanopowder for comparison. The %R was obtained using an integrated sphere in the spectrophotometer. As shown in this figure, the commercial pure TiO<sub>2</sub> nanopowder has high reflectivity in the visible-light region because of the wide energy band gap of pure-TiO<sub>2</sub> with 80% anatase-TiO<sub>2</sub> and 20% rutile-TiO<sub>2</sub>. It has an absorption edge at a wavelength around 390 nm that corresponds to energy band gap of around 3.18 eV. The synthesized Al-doped TiO<sub>2</sub> nanopowder also has extremely low diffuse reflectivity %R as much as commercial pure-TiO<sub>2</sub> nanopowder in ultraviolet region, and has lower reflectivity than commercial pure-TiO<sub>2</sub> nanopowder in the visible-light region. For the synthesized Al-doped TiO<sub>2</sub> nanopowder, the diffuse reflectivity %R in the visible-light region decreases with reduced SCL from 80% to 60%. The important point in the diffuse reflectivity is that synthesized nanopowder has an absorption edge at a wavelength around 400 nm. This wavelength of the absorption edge corresponds to an energy gap of 3.10 eV. On the other hand, %R for Al-doped TiO<sub>2</sub> nanopowder in the visible-light region decreases with reduced SCL from 80% to 60%. This reason was considered that Al concentration

in the vicinity of TiO<sub>2</sub> nanoparticle surface was probably changed depending on the SCL value[28]. This result suggests that Al doping to TiO<sub>2</sub> crystal can be done in the synthesized nanopowder using our PMITP-TCFF method. It is noteworthy that the production rate of Al-doped TiO<sub>2</sub> nanopowder was estimated as 400 g h<sup>-1</sup>.

## 5. Conclusions

Large amounts of Al-doped TiO<sub>2</sub> nanopowder were synthesized using pulse-modulated induction thermal plasmas (PMITP) with time-controlled feeding of feedstock (TCFF). The PMITP-TCFF method originally developed in our group, is characterized by the intermittent powder feeding synchronized with the modulated power of the PMITP. Effects of the coil current modulation degree were also studied for the synthesized Al-doped TiO<sub>2</sub> nanopowder. Results show that most of the synthesized powder had diameter of less than 100 nm. The diameter can be decreased by setting a reduced shimmer current level of the PMITP. The synthesized nanopowder was analyzed using several different methods including EDX, XRD, XPS, and spectrophotometry. Results showed that Al elements can be doped on TiO<sub>2</sub> nanopowder synthesized using the PMITP-TCFF method. The final production rate was estimated as higher than 400 g h<sup>-1</sup>.

## Acknowledgments

The authors would like to express their gratitude to Associate Professor Maria Antoaneta Bratescu, Mr Hoon-Seung Lee and Professor Nagahiro Saito at Nagoya University for helpful suggestions and comments related to BF-TEM and TEM/EDX mapping analysis.

This study was in part supported by Grant-in-Aid for Scientific Research (KAKENHI) (A) (23246050), The Japan Society for the Promotion of Science (JSPS), Japan, and by Adaptable and Seamless Technology Transfer Program through Target-driven (A-STEP) R&D (AS242Z01379M), Japan Science and Technology Agency (JST), Japan

## References

- [1] Malato S, Blanco J, Alarcon D C, Maldonado M I, Fernandez-Ibanez P and Gernjak W 2007 Photocatalytic decontamination and disinfection of water with solar collectors. *Catalysis Today* **122** 137–49
- [2] Li J, Zhao X, Wei H, Gu Z Z, and Lu Z 2008 Macroporous ordered titanium dioxide (TiO<sub>2</sub>) inverse opal as a new label-free immunosensor. *Analytica Chimica Acta* **625** 63–9
- [3] Gratzel M 2001 Photoelectrochemical cells. *Nature* **414** 338–44
- [4] Biju K P and Jain M K 2008 Effect of crystallization on humidity sensing properties of sol-gel derived nanocrystalline TiO<sub>2</sub> thin films. *Thin Solid Films* **516** 2175–80
- [5] Park J H, Park O O, and Kim S 2006 Photoelectrochemical water splitting at titanium dioxide nanotubes coated with tungsten trioxide. *Appl. Phys. Lett.* **89** 163106
- [6] Tsai Y C, Hsi C H, Bai H, Fan S K and Sun D H 2012 Single-step synthesis of Al-doped TiO<sub>2</sub> nanoparticles using non-transferred thermal plasma torch. *Jpn. J. Appl. Phys.* **51** 01AL01
- [7] Shon K H, Cho L D, Na H S, Kim B J, Park J H and Kim H J 2009 Development of a novel method to prepared Fe- and Al-doped TiO<sub>2</sub> from wastewater. *J. Ind. Eng. Chem.* **15** 476–82
- [8] Barolo G, Livraghi S, Chiesa M, Cristina M, Paganini C and Giamello E 2012 Mechanism of the photoactivity under visible light of N-doped titanium dioxide. charge carries migration in irradiated N-TiO<sub>2</sub> investigated by electrn paramagnetic resonance. *J. Phys. Chem. C* **116** 20887–94
- [9] Lee K N, Kim Y, Lee C W and Jai-Sung Lee J S 2011 Simultaneous amination of TiO<sub>2</sub> nanoparticles in the gas phase synthesis for bio-medical applications *Mater. Sci. Eng.* **18** 082021
- [10] Mio M, Kogoma M, Fukui H, and Kogoma A 2010 Control of inflammation using adsorption of inflammatory by nano-particles *Chem. Eng.* **55** 603-8
- [11] Girshick S L, Chiu C P, Munro R, Wu C Y, Yang L, Singh S K, and McMurry P H 1993 Thermal plasma synthesis of ultrafine iron particles. *J. Aerosol Sci.* **24** 367–82
- [12] Shigeta M, Watanabe T, and Nishiyama H 2004 Numerical investigation for nano-particle synthesis in an RF inductively coupled plasma. *Thin Solid Films* **457** 192–200
- [13] Oh S M and Ishigaki T 2004 Preparation of pure rutile and anatase TiO<sub>2</sub> nanopowders using RF thermal plasma. *Thin Solid Films* **457** 186–91
- [14] Lee J E, Oh S M, and Park D W 2004 Synthesis of nano-sized Al doped TiO<sub>2</sub> powders using thermal plasma. *Thin Solid Films* **457** 230–4
- [15] Ishigaki T, Oh S M, Li J G, and Park D W 2005 Controlling the synthesis of TaC nanopowders by injecting liquid precursor into RF induction plasma. *Sci. & Technol. Advanced Mater.* **6** 111–8
- [16] Tong L and Reddy R G 2006 Thermal plasma synthesis of SiC nano-powders/nano-fibers. *Materials Research Bulletin* **41** 2303–10
- [17] Ishigaki T and Li J G 2007 Synthesis of functional nanocrystallites through reactive thermal plasma processing. *Sci. & Technol. Advanced Mater.* **8** 617–23
- [18] Li J G, Ikeda M, Ye R, Moriyoshi Y, and Ishigaki T 2007 Control of particle size and phase formation of TiO<sub>2</sub> nanoparticles synthesized in RF induction plasma. *J. Phys. D: Appl. Phys.* **40** 2348–53
- [19] Tanaka Y, Nagumo T, Sakai H, Uesugi Y, and Nakamura K 2010 Nanoparticle synthesis using high-powered pulse-modulated induction thermal plasma. *J. Phys. D: Appl. Phys.* **43** 265201
- [20] Tanaka Y, Sakai H, Tsuke T, Uesugi Y, Sakai Y, and Nakamura K 2011 Influence of coil current modulation on TiO<sub>2</sub> nanoparticle synthesis using pulse-modulated induction thermal plasmas. *Thin Solid Films* **519** 7100–05
- [21] Tanaka Y, Tsuke T, Guo W, Uesugi Y, Ishijima T, Watanabe S, and Nakamura K 2012 A large amount synthesis of nanopowder using modulated induction thermal plasmas synchronized with intermittent feeding of raw materials. *J. Phys. D: Conf. Ser.* **406** 012001
- [22] Tanaka Y, Sakai H, Tsuke T, Guo W, Uesugi Y, Sakai Y and Nakamura K 2011 Nanoparticle synthesis using high-power modulated induction thermal plasmas with intermittent synchronized

- feeding of raw materials. *Proc. 20th Int. Symp. Plasma Chem. ISPC-20*, 346, Philadelphia, USA
- [23] Tanaka Y and Sakuta T 2003 Temperature control of Ar induction thermal plasma with diatomic molecular gases by pulse-amplitude modulation of coil current. *Plasma Sources Sci. & Technol.* **12** 69–77
- [24] Tanaka Y, Uesugi Y, and Sakuta T 2007 Controlling the number of excited atoms flowing into the reaction chamber using pulse-modulated induction thermal plasmas at atmospheric pressure. *Plasma Sources Sci. & Technol.* **16** 281–9
- [25] Ohno T, Sarukawa K, Tokieda K, and Matsumura M 2001 Morphology of a TiO<sub>2</sub> photocatalyst (degussa, P-25) consisting of anatase and rutile crystalline phases. *J. of Catal.* **203** 82–6
- [26] Tanaka Y, Guo W, Kodama N, Uesugi Y, Sakai Y and Nakamura K 2013 A novel approach for large amount synthesis of TiO<sub>2</sub> nanopowder using modulated induction thermal plasmas with time-controlled feeding of feedstock. *Proc. 21th Int. Symp. Plasma Chem. ISPC-21*, OR **52**, Cairns, Australia
- [27] Abazović N D, Mirengli L, Janković I A, Bibić N, Šojić D V, Abramović B F and Čomor M I 2009 Synthesis and characterization of rutile TiO<sub>2</sub> nanopowders doped with iron ions. *Nanoscale Res. Lett.* **4** 518–25
- [28] Trejo-Tzab R, Alvarado-Gil J J, Quintana P, Bartolo-Pérez P 2012 N-doped TiO<sub>2</sub> P25/Cu powder obtained using nitrogen(N<sub>2</sub>) gas plasma. *Catal. Today* **193** 179–85

**Table 1.** Experimental conditions.

Time-averaged input power	20 kW
Fundamental frequency of the coil current	450 kHz
Modulation cycle	15 ms
Shimmer current level, SCL	60%, 70%, 80%
Modulation time	15 ms
Duty factor, DF	80% (On-time / Off-time = 12 ms / 3 ms)
Pressure	300 torr (= 40 kPa)
Gas composition	Ar: 90 L min <sup>-1</sup> , O <sub>2</sub> : 10 L min <sup>-1</sup>
Carrier gas flow rate	Ar: 4 L min <sup>-1</sup>
Quenching gas flow rate	Ar: 50 L min <sup>-1</sup>
Open and close time of solenoid valve	12 ms for open and 3 ms for close
Delay time of solenoid valve open $t_d$	6 ms
Powder feed rate $g_{pow}$	19 g min <sup>-1</sup> for 60%SCL, 12 g min <sup>-1</sup> for 70%SCL and 80%SCL
Raw powder and its maximum size	95wt%Ti + 5wt%Al, $\bar{d}_{Ti} = 27 \mu\text{m}$ , $d_{Ti} < 45 \mu\text{m}$ $\bar{d}_{Al} = 3 \mu\text{m}$

## Figure captions

**Figure 1.** Modulated coil current and definition of modulation parameters.

**Figure 2.** Method for large-scale nanopowder synthesis using pulse-modulated induction thermal plasma with time-controlled feedstock feeding (PMITP-TCFF).

**Figure 3.** Whole system of nanopowder synthesis using PMITP-TCFF.

**Figure 4.** FE-SEM images for (a) feedstock, and synthesized powder with conditions (b) 80%SCL,  $g_{\text{pow}} = 12 \text{ g min}^{-1}$ , (c) 70%SCL,  $g_{\text{pow}} = 12 \text{ g min}^{-1}$ , and (d) 60%SCL,  $g_{\text{pow}} = 19 \text{ g min}^{-1}$ .

**Figure 5.** Particle size distributions for (a) 80%SCL,  $g_{\text{pow}} = 12 \text{ g min}^{-1}$ , (b) 70%SCL,  $g_{\text{pow}} = 12 \text{ g min}^{-1}$ , and (c) 60%SCL,  $g_{\text{pow}} = 19 \text{ g min}^{-1}$ .

**Figure 6.** Dependence of particle mean diameter and standard deviation on the shimmer current level of the pulse modulation.

**Figure 7.** BF-TEM and TEM/EDX mapping for (a) 80%SCL,  $g_{\text{pow}} = 12 \text{ g min}^{-1}$ , (b) 70%SCL,  $g_{\text{pow}} = 12 \text{ g min}^{-1}$ , and (c) 60%SCL,  $g_{\text{pow}} = 19 \text{ g min}^{-1}$ .

**Figure 8.** XRD spectra for (a) 80%SCL,  $g_{\text{pow}} = 12 \text{ g min}^{-1}$ , (b) 70%SCL,  $g_{\text{pow}} = 12 \text{ g min}^{-1}$ , (c) 60%SCL,  $g_{\text{pow}} = 19 \text{ g min}^{-1}$ , and (d) reference peaks.

**Figure 9.** XPS spectra for commercial pure-TiO<sub>2</sub> (P-25; Degussa), pure-TiO<sub>2</sub> nanopowder synthesized using PMITP-TCFF and Al-doped TiO<sub>2</sub> nanopowder synthesized in this study. (a) Ti 2p region between 455 eV and 470 eV, (b) Al 2p region between 70 eV and 80 eV.

**Figure 10.** Diffuse reflection spectra for commercial pure-TiO<sub>2</sub> (P-25; Degussa) and Al-doped TiO<sub>2</sub> nanopowder synthesized in this study.

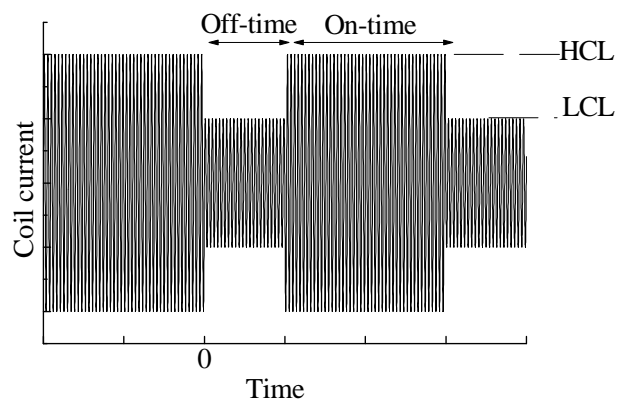


**Figure 1.** Modulated coil current and definition of modulation parameters.

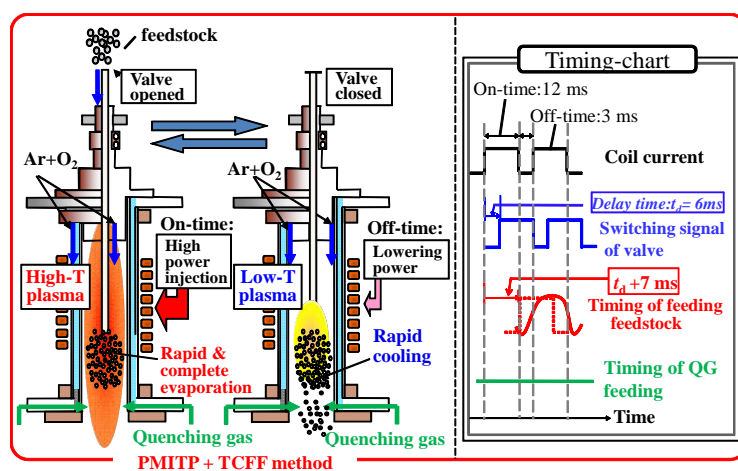


**Figure 2.** Method for large-scale nanopowder synthesis using pulse-modulated induction thermal plasma with time-controlled feedstock feeding (PMITP-TCFF).

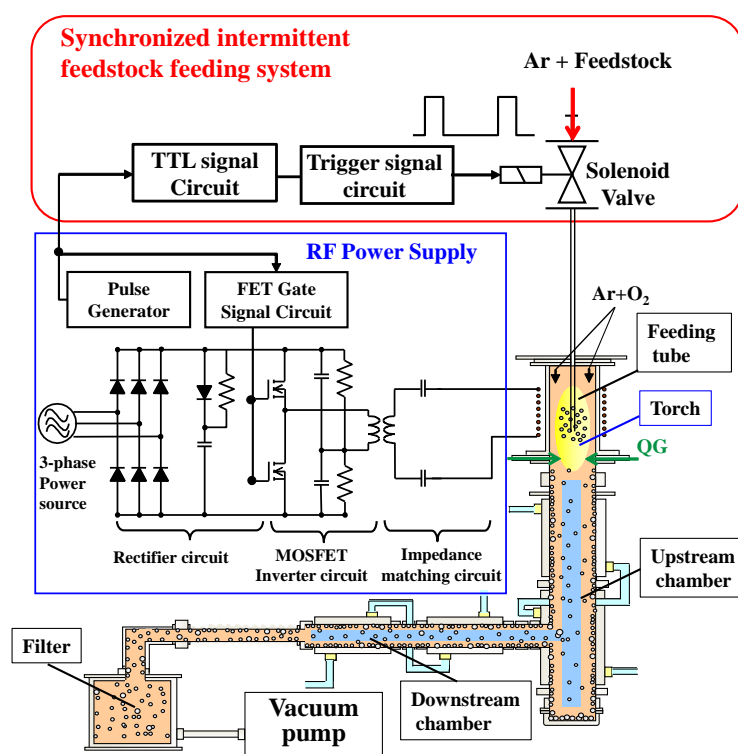
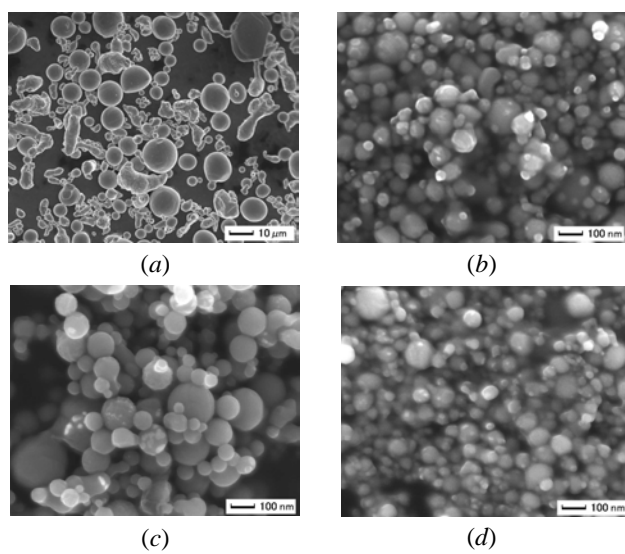
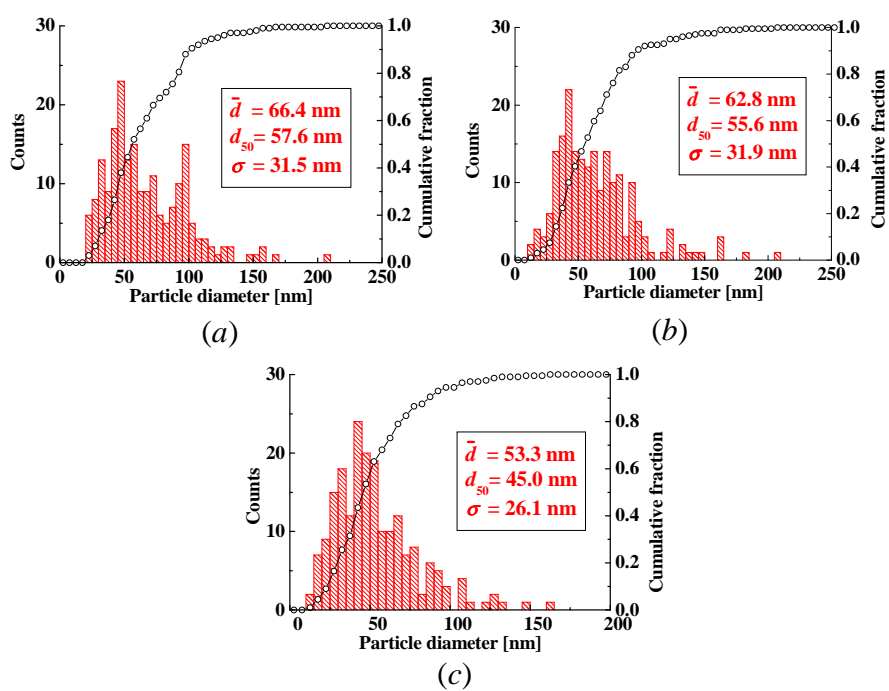


Figure 3. Whole system of nanopowder synthesis using PMITP-TCFF.



**Figure 4.** FE-SEM images for (a) feedstock, and synthesized powder with conditions (b) 80%SCL,  $g_{\text{pow}} = 12 \text{ g min}^{-1}$ , (c) 70%SCL,  $g_{\text{pow}} = 12 \text{ g min}^{-1}$ , and (d) 60%SCL,  $g_{\text{pow}} = 19 \text{ g min}^{-1}$ .



**Figure 5.** Particle size distributions for (a) 80%SCL,  $g_{\text{pow}} = 12 \text{ g min}^{-1}$ , (b) 70%SCL,  $g_{\text{pow}} = 12 \text{ g min}^{-1}$ , and (c) 60%SCL,  $g_{\text{pow}} = 19 \text{ g min}^{-1}$ .

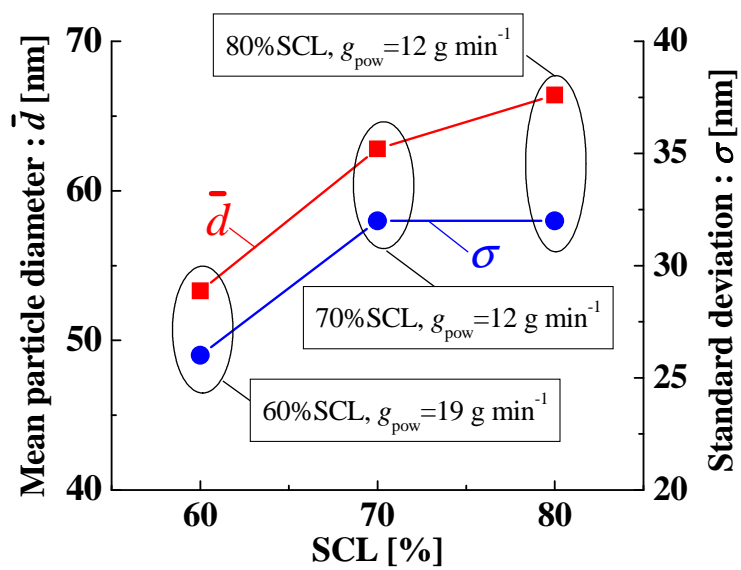


**Figure 6.** Dependence of particle mean diameter and standard deviation on the shimmer current level of the pulse modulation.

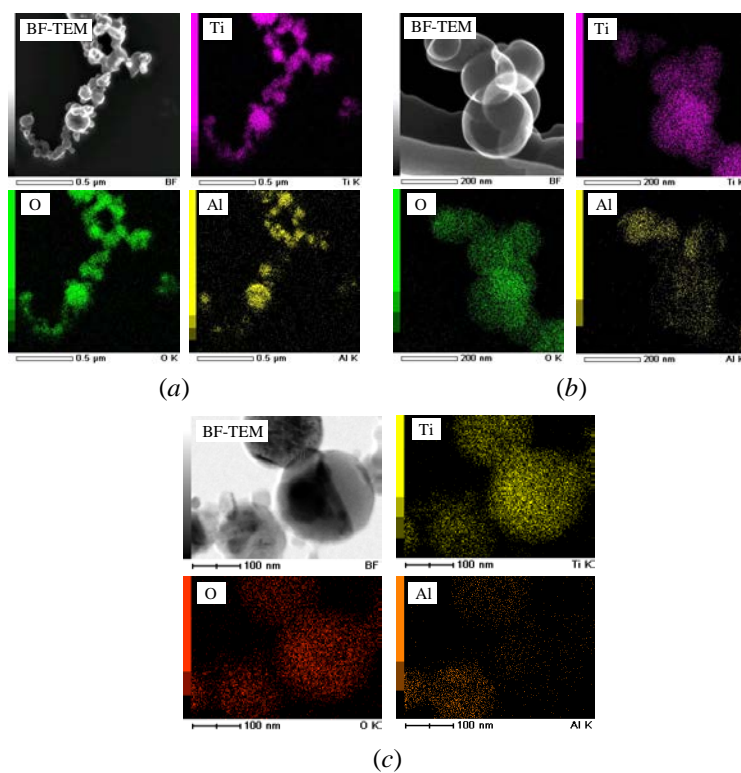


**Figure 7.** BF-TEM and TEM/EDX mapping for (a) 80%SCL,  $g_{pow} = 12 \text{ g min}^{-1}$ , (b) 70%SCL,  $g_{pow} = 12 \text{ g min}^{-1}$ , and (c) 60%SCL,  $g_{pow} = 19 \text{ g min}^{-1}$ .

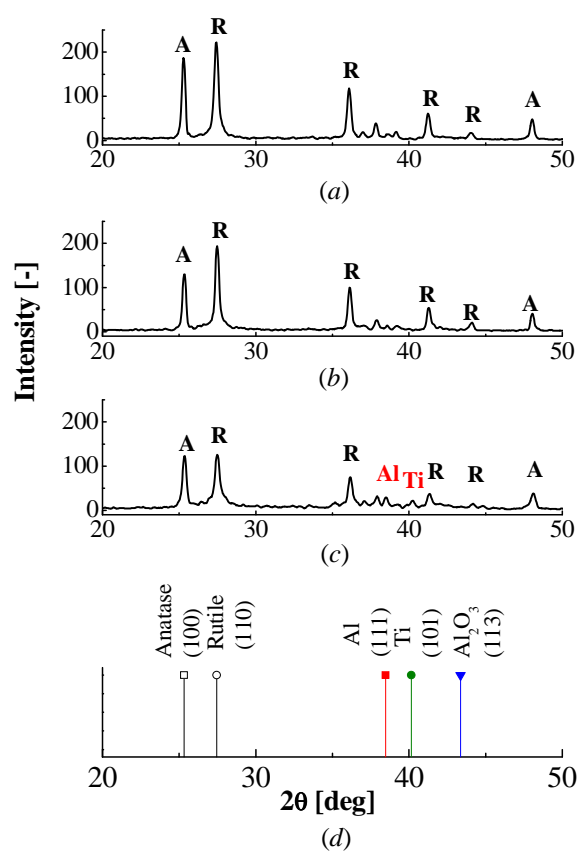


**Figure 8.** XRD spectra for (a) 80%SCL,  $g_{\text{pow}} = 12 \text{ g min}^{-1}$ , (b) 70%SCL,  $g_{\text{pow}} = 12 \text{ g min}^{-1}$ , (c) 60%SCL,  $g_{\text{pow}} = 19 \text{ g min}^{-1}$ , and (d) reference peaks.

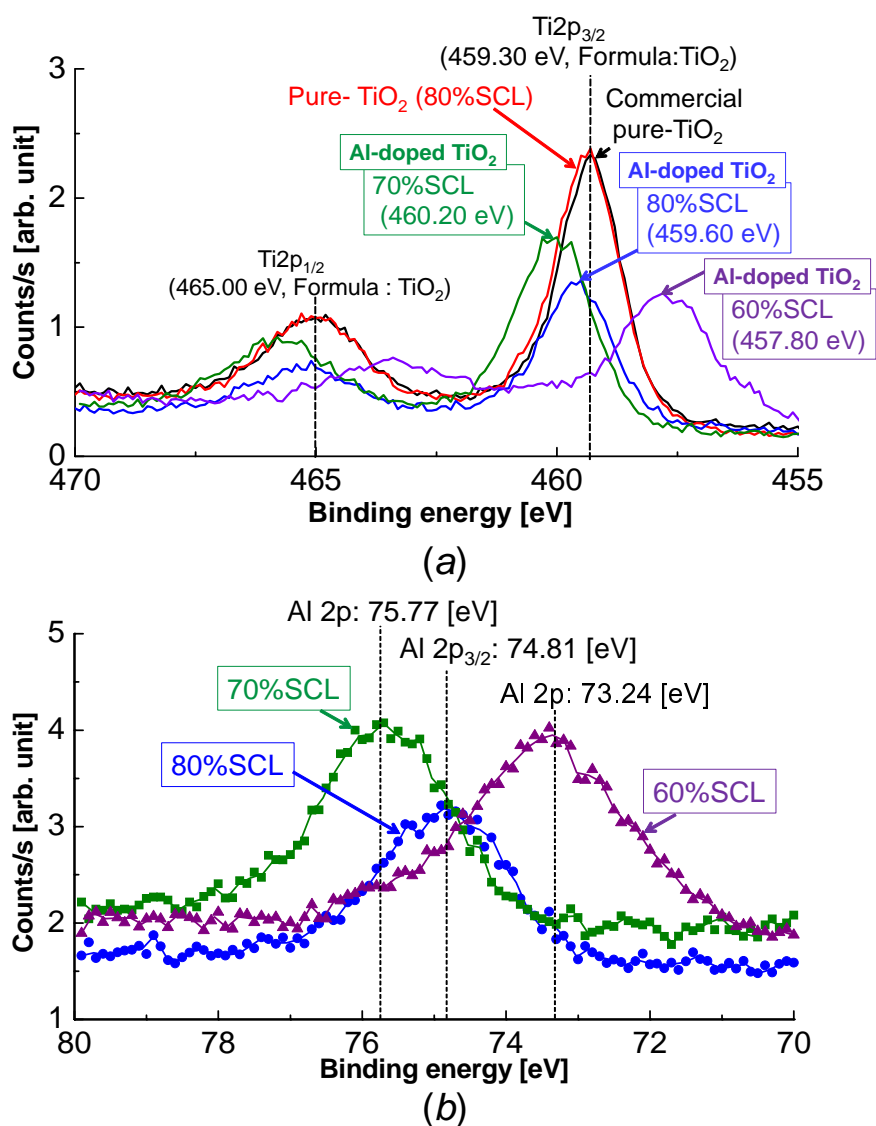


**Figure 9.** XPS spectra for commercial pure-TiO<sub>2</sub> (P-25; Degussa), pure-TiO<sub>2</sub> nanopowder synthesized using PMITP-TCFF and Al-doped TiO<sub>2</sub> nanopowder synthesized in this study. (a) Ti 2p region between 455 eV and 470 eV, (b) Al 2p region between 70 eV and 80 eV.

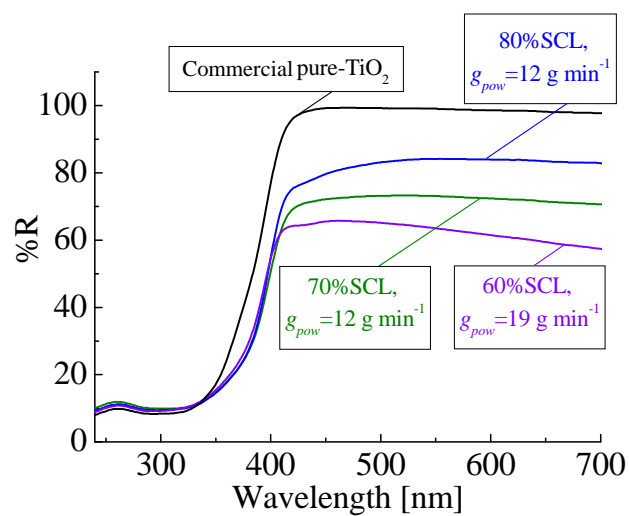


**Figure 10.** Diffuse reflection spectra for commercial pure-TiO<sub>2</sub> (P-25; Degussa) and Al-doped TiO<sub>2</sub> nanopowder synthesized in this study.